

# Feasibility Study and Conceptual Design of Missile-Borne Synthetic Aperture Radar

Jamal Saeedi, *Member, IEEE*

**Abstract**—In this paper, feasibility study along with conceptual design of missile-borne synthetic aperture radar (SAR) has been accomplished, which can effectively improve the detection capability and the blow precision of a missile. First, SAR echo signal modeling, geometry configuration for missile-borne SAR scenario, and an appropriate image formation algorithm are presented. Then, a system block diagram along with complete discussions about different parts and system design considerations of the SAR seeker are explained. Finally, simulation of the whole system along with raw data generation considering the imaging geometry of the missile-borne SAR seeker has been performed. Experimental results show that the proposed system is capable of imaging and targeting in the complicated geometry of missile-borne SAR.

**Index Terms**—Missile-borne, raw data generation, seeker, synthetic aperture radar (SAR), system design considerations.

## I. INTRODUCTION

A SEEKER is considered as the eye of a missile, and its job is to obtain and track the target until the missile hits the target. A missile's guidance system can be divided into the infrared, laser, radar seekers, etc. Because the propagation loss of infrared, laser, and visible light in the atmosphere is much larger than the microwave band and the transmission distance limitation, the radar seeker has become the dominant development for seekers. In addition, for a mission where the target area is covered by clouds, selecting a seeker which is capable of seeing through the clouds is a key factor. Radar seekers have a clear benefit over cloud blind electro-optical seekers. The guidance scheme and target type are the biggest factors that influence the seeker design choice. In this paper, the guidance scheme is selected to be a synthetic aperture radar (SAR) system, and target type is a ship.

SAR is an imaging technique that produces high-resolution maps of the radar cross section (RCS) of a scene by processing the coherent phase history of the echoed signal over transmitting of multiple pulses. It is the only effective sensor which has the capability of operation on a day/night basis and in all weather conditions, and it produces images with high resolution [1], [2].

Manuscript received October 22, 2016; revised April 4, 2017; accepted June 15, 2017. This paper was recommended by Associate Editor W. Shen.

The author is with the Electrical Engineering Department, Amirkabir University of Technology, Tehran 15875-4413, Iran (e-mail: jamal.saeedi@yahoo.com).

Color versions of one or more of the figures in this paper are available online at <http://ieeexplore.ieee.org>.

Digital Object Identifier 10.1109/TSMC.2017.2718114

A SAR seeker can obtain the missile's position errors relative to planned trajectory by matching the real-time image with the prepared reference image. Then the obtained precise position parameters can be used to correct the accumulated drift errors and initialized geo-location errors of inertial guidance system (INS), which effectively improves the guidance precision and attack ability of the medium-long range missiles [3], [4]. However, the missile-borne SAR as compared with the airborne and space-borne systems is faced with many complex problems brought by missile's maneuverable dynamics such as vertical dive. Compared with the traditional air-borne SAR, the missile-borne SAR has important characteristics including high flight speed, nonstraight movement with nonconstant velocity, and high squint angle, which forward a greater requirement for precision processing and imaging. In this paper, the objective is to design a new missile-borne SAR seeker to cope with these challenges.

The earliest information on the Internet related to the SAR seeker is from the U.S. Government website [5], which is an awarded project in 1987. Because of the importance of SAR seeker as one of the missile's eye, there is no useful technical information related to this project on the Internet, unlike the conventional air-borne SAR systems. Content on the Internet related to the SAR seeker can be divided into three categories: 1) military products; 2) papers; and 3) patents. Joint air-to-surface standoff missile can be mentioned among the different missiles in which a SAR seeker is used [6]. There are also reports that claim China used SAR seeker technology in their antiship ballistic missiles [7]. Existing papers generally deal with signal modeling and processing with respect to the special geometry of missile. For example, in [8] raw signal modeling for missile-borne SAR is performed. In addition, in [9] an algorithm for flight trajectory optimization in order to get an image with good quality from SAR seeker is proposed. An appropriate system design considerations for SAR seeker can be mentioned among the issues that are not available in these kind of articles. In the case of patents, only one similar case for SAR seeker is found, which is used for air-to-ground missile guidance [10]. In this case, a squint imaging geometry using SAR sensor is considered, and different parts of SAR seeker together with the general description are given.

The proposed missile-borne SAR seeker has been designed in the monostatic imaging mode. In general, SAR sensors can be used in two different modes for imaging: 1) monostatic and 2) bistatic. Imaging in flight direction or backward is the most important advantage of a bistatic system compared to a monostatic one. Monostatic SAR typically operates

with a side-looking antenna to obtain high-resolution images. However, in the case of imaging in forward- and backward-looking directions for monostatic SAR, left/right ambiguity occurs [11]. Although, using SAR system in the bistatic mode as missile's seeker would be a perfect choice; but it creates more complications in terms of design and construction, and it will considerably increase the cost as compared to the monostatic case. One simple solution to avoid the bistatic option is to use the conventional monostatic in squint mode in order to cover forward direction as much as possible and enlarge the search area for missile. Two major challenges for forward-looking SAR imaging are left/right ambiguity and low Doppler (azimuth) resolution [11]. Ender [11] showed that the azimuth resolution on the earth surface is related to gradient of the Doppler frequency. Since, the gradient of the Doppler frequency in the flight direction is very small, the Doppler resolution obtained with forward-looking SAR imaging is therefore extremely low. On the other hand, the ground-range resolution  $\delta_{gr}$  is inversely proportional to the sinusoid of the grazing angle  $\gamma$ , i.e.,  $\delta_{gr} = \delta_r / \sin \gamma$ , where  $\delta_r$  is slant range resolution; therefore it will be worsen in angles near to nadir direction. This is more problematic for missile-borne SAR case as compared to the conventional airborne SAR. In the squint mode SAR imaging, since the altitude of missile-borne SAR is too high, the angle between the grazing angle and the nadir line is close to zero, so the ground-range resolution is to be drastically reduced. These are the problems concerns with monostatic SAR seeker that should be considered in the system design. Nonetheless, the resolution issue for missile-borne SAR seeker is not as much problematic as compared to the conventional high-resolution SAR imaging. This is because the missile-borne SAR seeker is considered here in the context of positioning and targeting sea targets as opposed to high-resolution imaging.

The remainder of this paper is organized as follows. The proposed method for SAR seeker along with system block diagram and signal modeling are explained in Section II. System design considerations for missile-borne SAR are discussed in Section III. Section IV illustrates results of feasibility study based on the system design with raw data simulation of a ship model. Finally, the conclusions are given in Section V.

## II. PROPOSED MISSILE-BORNE SAR SEEKER

In this section, the general framework of the proposed missile-borne SAR seeker as well as signal modeling and image formation algorithm will be discussed. The SAR seeker here will be considered as the terminal guidance for an anti-ship ballistic missile. A ballistic missile goes up to very high peak using propulsion engine, and then move toward the target using gravity and proper guidance during the return path. The missile's motion is a motion with variable speed and acceleration. The terminal guidance phase will typically involve the last minute of the flight, about 40-km range, and will require the accurate determination of the target location and information about the optimal approach route to the target.

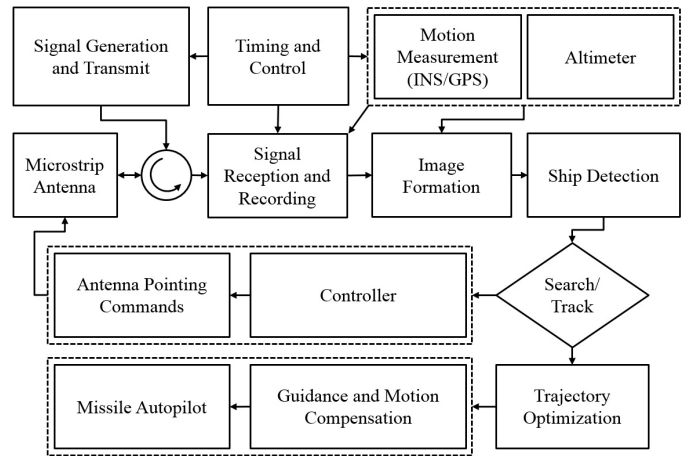


Fig. 1. Block diagram of the proposed SAR seeker.

A SAR seeker will be used in conjunction with global positioning system (GPS) and INS updates to determine the target location.

### A. System Block Diagram

The block diagram for the proposed SAR seeker is shown in Fig. 1. In the following, we have briefly described about different subsystems of the SAR seeker. The separate subsystems must work closely together for the SAR seeker to operate correctly.

1) *Timing and Control*: The SAR signal must be coherent over the entire series of pulses to form an image with good quality. To aim this, coherency and consistent timing between the separate subsystems of the SAR system must be maintained. Specifically, the timing and control system maintains coherency from pulse to pulse and between subsystems and determines the timing for turning the radar on and off or switching between transmit and receive modes.

2) *Signal Generation and Transmit*: Commonly, the SAR signal is generated at baseband and then mixed up to the selected operating frequency before going through antenna. The antenna is designed with specific beamwidths (in azimuth and elevation) and can be pointed out in different directions for different SAR imaging modes.

3) *Signal Reception and Recording*: After transmitting the amplified signal through the antenna to the target area, a very small portion of it reflects back to the radar antenna. For monostatic operation, the radar echoes are received through the transmit antenna which is isolated from the transmit path by a circulator. The received signal is amplified with a low-noise amplifier (LNA) and mixed-down to an appropriate frequency band for sampling.

4) *Motion Measurement*: SAR processing requires information of the flight path during data collection. Motion measurement system used with the missile-borne SAR system employs a high rate INS coupled with GPS and carefully time-tagged and aligned with the collected SAR data. It should also be accompanied by an altimeter system for better targeting of missile.

5) *Image Formation*: SAR processing algorithm usually includes three main steps to appropriately focus the data consisting of range compression, range cell migration correction (RCMC), and azimuth compression. It is also accompanied by a motion compensation step for phase error compensation caused by nonlinear flight trajectory.

6) *Ship Detection*: In terminal guidance, the real-time images provided by missile-borne SAR are matched with the target reference templates stored in the memory. The matched results are used to guide the missile to precisely attack the target [12]–[14].

7) *Search/Track*: The initial mode of SAR seeker is search mode in which the SAR antenna is illuminated to possible target areas using gimbal and control commands. After the ship is detected using a proper target identification technique, the track mode will begin [15]. At this stage, the INS accumulated error will be compensated and a suitable optimized route toward target is provided for missile automatic flight control system. The reason for doing the trajectory optimization is that the SAR seeker would be able to track the target and not the so-called blind.

8) *Trajectory Optimization*: After the ship detection step, the missile must appropriately move toward the target in the track mode to able the SAR seeker for producing good resolution images. The imaging resolution of missile-borne SAR is not only related with SAR parameters but also with flight trajectory and look angle. As the missile imaging time is limited, in order to get the best resolution, the missile curve trajectory must be designed and optimized [9], [16]–[18].

In this paper, we have concentrated on signal modeling and image formation algorithm for imaging geometry of missile-borne SAR, which will be described in the remaining of this section. It should be mentioned that ship detection and missile trajectory optimization are beyond the scope of this paper; however, system design considerations, which deals with choosing SAR system parameters, will be explained in the next section.

### B. Echo Signal Modeling and Geometry Configuration

This section presents the fundamentals of SAR signal modeling and geometry configuration for missile-borne SAR scenario. Before the SAR signal is generated, a number of important system parameters should be determined, including carrier frequency, bandwidth, pulse length, and pulse repetition frequency (PRF). The transmitted signal is a linear frequency modulated (LFM) waveform, where the signal spans the bandwidth over the pulse length. This cycle is repeated at the PRF. The LFM transmit signal at RF band can be expressed as

$$s_t(t) = A(t) \exp\left(j\left(2\pi f_0 t + \pi k_r t^2 + \varphi_0\right)\right) \quad (1)$$

where  $A(t)$  is the signal amplitude and defines the pulse length with a rectangular function,  $f_0$  is the frequency at the beginning of the chirp,  $k_r$  is chirp rate, and  $\varphi_0$  is the starting phase which can usually be neglected.

A power amplifier increases the signal power to a specified level in the transmission chain. An antenna propagates the amplified signal to the target area. A very small portion of transmitted signal reflects back to the radar antenna. The

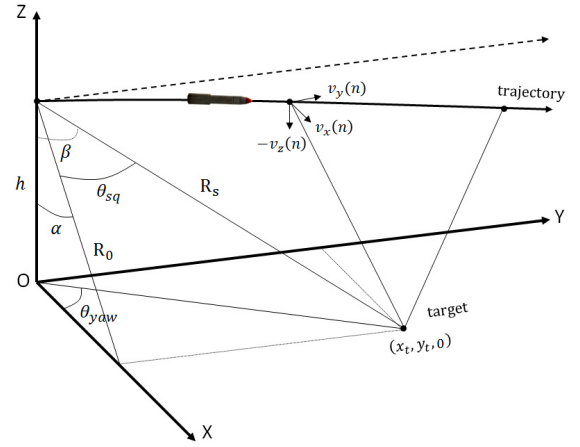


Fig. 2. Missile-borne SAR geometry.

echoed signal from target can be expressed as

$$s_r(t, \eta) = A'(t) \exp\left(j\left(2\pi f_0(t - \tau) + \pi k_r(t - \tau)^2\right)\right) \quad (2)$$

where  $t$  is the fast time,  $\eta$  is the azimuth time, and  $A'(t)$  is an weakened version of  $A(t)$ , and  $\tau$  is the two-way time of flight to the target at range  $R$  expressed as

$$\tau = 2R(\eta)c_0 \quad (3)$$

where  $c_0$  is light speed.

The received signal is amplified with an LNA and mixed down to an appropriate band for sampling. After the signal from (2) is mixed down by a frequency,  $f_m$ , the signal ready to be recorded is as

$$s_{\text{rmd}}(t) = A''(t) \exp\left(j\left(2\pi(f_0 - f_m)t + \pi k_r(t - \tau)^2 - 2\pi f_0 \tau\right)\right) \quad (4)$$

where  $A''(t)$  is an amplified version of  $A'(t)$ .

For simplification let  $f_m = f_0$ , therefore

$$s_{\text{rm}}(t, \eta) = A''(t) \exp\left(j\left(-2\pi f_0 \tau + \pi k_r(t - \tau)^2\right)\right). \quad (5)$$

SAR system digitize this data and process it on-board to form image for ship detection step. In the following, the geometry configuration for the missile-borne SAR is described in details, and then appropriate signal processing algorithm for SAR image formation will be explained in the next section.

The geometry configuration for the missile-borne SAR in squint stripmap mode is shown in Fig. 2. In this paper, we suppose that the missile is diving with constant acceleration during the coherent processing interval. At the azimuth time (slow time)  $\eta = 0$ , the projection of radar location on the ground is assumed to be the origin of Cartesian coordinates OXYZ and  $h$ ,  $v = (v_x, v_y, -v_z)$ , and  $a = (a_x, a_y, -a_z)$  denote the height, the velocity vector, and the acceleration vector of the radar platform, respectively.

The point  $(x_t, y_t, 0)$  denotes a distortionless isotropic point scatterer in the ground surface. Therefore, the relative slant-range vector from the radar to the target at  $\eta = 0$  is as follows:

$$R_s = \sqrt{x_t^2 + y_t^2 + h^2}. \quad (6)$$

From the geometry shown in Fig. 2, one can get the following relations for *squint* and *incident* angles:

$$\theta_{\text{sq}} = \arctan\left(\frac{x_t}{R_0}\right) = \arctan\frac{\tan(\theta_{\text{yaw}})\tan(\alpha)}{\sqrt{1 + \tan^2(\alpha)}} \quad (7)$$

$$\beta = \arctan\left(\tan(\alpha)\sqrt{\tan^2(\theta_{\text{yaw}}) + 1}\right) \quad (8)$$

where  $R_0 = \sqrt{y_t^2 + h^2}$ ,  $\theta_{\text{yaw}} = \arctan(x_t/y_t)$ ,  $\alpha = \arctan(y_t/h)$ , and  $\beta = \arctan(\sqrt{y_t^2 + x_t^2}/h)$ .

Then, the slant range between the radar platform and the target over azimuth time,  $\eta$  is as follows:

$$R_s = \sqrt{(x_t - x_s(\eta))^2 + (y_t - y_s(\eta))^2 + (h - z_s(\eta))^2} \quad (9)$$

where  $x_s(\eta)$ ,  $y_s(\eta)$ , and  $z_s(\eta)$  are defined as

$$\begin{aligned} x_s(\eta) &= v_x\eta + \frac{1}{2}a_x\eta^2, & y_s(\eta) &= v_y\eta + \frac{1}{2}a_y\eta^2 \\ z_s(\eta) &= v_z\eta + \frac{1}{2}a_z\eta^2. \end{aligned} \quad (10)$$

The following equation gives the scene center parameter,  $x_c$ , based on the geometry of the missile-borne SAR shown in Fig. 2:

$$x_c = h\tan(\alpha). \quad (11)$$

Then using a specific yaw angle,  $\theta_{\text{yaw}}$ , we can obtain another scene center parameter,  $y_c$ , as

$$y_c = \sqrt{R_s^2 - R_0^2}. \quad (12)$$

Using (11) and (12) we can obtain the *incident* angle,  $\beta$ , and also *squint* angle,  $\theta_{\text{sq}}$ . Then, maximum and minimum ranges can be obtained using antenna *elevation* angle,  $\theta_{\text{el}}$ , as follows:

$$R_{\min} = h\tan\left(\beta + \frac{\theta_{\text{el}}}{2}\right), \quad R_{\max} = h\tan\left(\beta - \frac{\theta_{\text{el}}}{2}\right). \quad (13)$$

Based on the geometric relations obtained in this section as well as the echoed signal model in (5), one can simulate raw data for missile-borne SAR scenario. For this reason, system parameters as well as flight trajectory should be specified for well-functioning of missile-borne SAR seeker. In the following, the signal processing algorithm for image formation from the raw data is described.

### C. Image Formation Algorithm

The most frequently used SAR processing technique is the range-Doppler algorithm (RDA) [19]. The chirp-scaling algorithm was introduced to exclude the interpolation used for RCMC in the RDA [19]. Third processing method is recognized as the omega-K algorithm ( $\omega$ -K) [19]. In the  $\omega$ -K method, SAR raw data is processed in the 2-D frequency domain without any approximation in deriving the signal model, which makes it appropriate for high-squint mode SAR. The most general and computationally costly algorithm is known as back-projection (BP) [20]. The benefits of BP

include the simplicity of the algorithm, the parallel computation structure, and the ability to process data from an arbitrary platform path.

Two issues should be considered for selecting a proper signal processing algorithm for missile-borne SAR scenario: one is the squint imaging mode and the other one is nonlinear flight path of missile. With regards to these two issues and above discussion about different processing algorithms, one can conclude that BP algorithm is the best choice for processing of missile-borne SAR raw data. In the following, the theory related to the BP processing algorithm is described. BP normally operates on the range-compressed data [20]. For SAR data, range compression can be performed using MF. Using the stop and go approximation,  $\tau_0$  does not depend in fast time  $t$ , and SAR image from a point target is formed using the following formula [20]:

$$\begin{aligned} \text{im}(x_0, y_0, z_0) &= \sum_{\eta} \exp(j2\pi f_0 \tau_0) \sum_t s_{\text{rm}}(t, \eta) \\ &\quad \times \exp\left(-j\pi k_r(t - \tau_0)^2\right) \end{aligned} \quad (14)$$

where  $(x_0, y_0, z_0)$  is the coordinate of the point target and  $\tau_0$  is obtained using the following:

$$\begin{aligned} \tau_0 &= 2R(t, \eta)/c_0 \\ &= 2\sqrt{(H - z_0)^2 + y_0^2 + (v(t + \eta) - x_0)^2}/c_0 \end{aligned} \quad (15)$$

where  $v$  is the platform velocity,  $H$  is the flight altitude, and  $c_0$  is the light speed.

The inner sigma in (14) is the definition of MF. For range compression, we define a reference chirp equal to the transmit signal. When the received signal is convolved with the reference chirp, the result is a peak where the signals line up. This peak corresponds to the target range. In processing, this is efficiently done with an FFT, a complex-phase multiply, and an inverse FFT

$$\begin{aligned} s_{\text{rc}}(\tau_0, \eta) &= \sum_t s_{\text{rm}}(t, \eta) \exp\left(-j\pi k_r(t - \tau_0)^2\right) \\ &\approx a \text{Sinc}(b(t - \tau_0)) \end{aligned} \quad (16)$$

where  $a$  and  $b$  are constants.

Using (16), (14) can be reformulated as

$$\text{im}(x_0, y_0, z_0) = \sum_{\eta} \exp(j2\pi f_0 \tau_0) s_{\text{rc}}(\tau_0, \eta). \quad (17)$$

### III. SYSTEM DESIGN CONSIDERATIONS

For the conventional airborne SAR, it is commonly assumed that the height, swath width, and velocity are constant or has multiple modes (in each mode these parameters are constant). While these parameters for the missile-borne SAR seeker undergone drastic changes. One of the problems arising from these changes is the phase error in the collected raw signal; however, one can use the information obtained by navigation system information to compensate the phase error. Another problem is the changes in altitude and speed of the missile-borne SAR, which force us to use different pulse width (PW) and PRF accordingly. This can also

TABLE I  
SYSTEM REQUIREMENTS FOR THE PROPOSED MISSILE-BORNE SAR

Parameter	Value
Operating Mode	Squint-Stripmap
Transmitted Waveform	LFM
Environment	Sea
Operational Altitude	5000-30000 m
Maximum Range	34000 m
Incident Angle	6-30 degree
Swath Width	1000-8000 m
Operational Velocity	$\leq 2000$ m/s
Antenna Dimensions	$\leq 17 \times 17$ cm <sup>2</sup>
Ground-Range Resolution	$\leq 10$ m
Cross-Range Resolution	$\leq 1$ m

be solved by using a variable PW and PRF system using a controller.

Before starting the designing steps, there should be initial requirements for the missile-borne SAR system. Table I outlines the system-level requirements. The imaging geometry is selected to be squint-stripmap. The application that we are looking for here is a SAR seeker for antiship ballistic missile; therefore, the imaging environment is sea area. The terminal guidance phase of the SAR seeker will typically involve the last minute of flight, about 30-km range; therefore we consider here altitude varies from 30 km to 5 km. Missile flight speed while imaging is another parameter that should be considered for designing. We have considered a maximum of 2000 m/s velocity of missile for minimum PRF determination in the design process. Another important factor is the size limit for mounting the SAR seeker antenna at the head of the missile. Here, we have considered an area of  $17 \times 17$  cm<sup>2</sup> as maximum antenna dimensions. Ground-range resolution is the final requirement for designing the SAR seeker. As we have discussed the application that we are looking for is an antiship ballistic missile, i.e., localization for targeting the ship is more important than a high-resolution image. Here, 10 m is chosen for ground-range resolution. The radar operational specifications are chosen based on these initial requirements. In the remainder of this section, the design process will be explained.

#### A. Operating Radar Frequency

SAR system can operate in wide frequency band from L-band to Ku-band. However, there are optimal ranges for various tasks. For radar frequency selection of missile-borne SAR to meet the initial requirements, the following factors should be considered: antenna dimensions, radio signals' attenuation in atmosphere, and targets' RCS variations. The detailed analysis of this notion is given below.

1) *Antenna Dimensions*: Now the analysis is done for the limitations caused by the hardware size. The longer is a wavelength, the bigger is the hardware size and weight. There is a rigid size requirement for the missile-borne SAR case as shown in Table I,  $17 \times 17$  cm<sup>2</sup>. Therefore, it should be considered here in order to determine possible frequency ranges. A microstrip patch array antenna is a good choice for antenna type because of its low weight, easy installation, and the ability to control the antenna pattern. For this kind

on antenna, the relationship between 3-dB antenna beamwidth and antenna length,  $L$ , is obtained as follows [21]:

$$\theta_{el}^{\circ} = \frac{60\lambda}{L_{el}} \quad \text{or} \quad \theta_{el}^{\text{rad}} = \frac{0.89\lambda}{L_{el}} \quad (18)$$

$$\theta_{az}^{\circ} = \frac{60\lambda}{L_{az}} \quad \text{or} \quad \theta_{az}^{\text{rad}} = \frac{0.89\lambda}{L_{el}} \quad (19)$$

where  $\lambda$  is wavelength,  $L_{el}$  is antenna length in elevation direction, and  $L_{az}$  is antenna length in azimuth direction.

Using (13), we can obtain the following relation for swath width and antenna elevation beamwidth:

$$\begin{aligned} \text{swath} &= R_{\max} - R_{\min} \\ &= h \tan\left(\beta - \frac{\theta_{el}}{2}\right) - h \tan\left(\beta + \frac{\theta_{el}}{2}\right) \end{aligned} \quad (20)$$

$$\theta_{el} = 2\left(\beta - a \tan\left(\tan(\beta) - \frac{\text{swath}}{2h}\right)\right). \quad (21)$$

Based on the initial requirements shown in Table I, to make a swath width of 1000 m at altitude of 5000 m, the antenna elevation beamwidth with an incident angle of 6° can be obtained as follows:

$$\theta_{el} = 2\left(6 - a \tan\left(\tan(6) - \frac{1000}{2.5000}\right)\right) = 11.41 \text{ degree.}$$

Since, the allowable antenna length in elevation direction is 17 cm; therefore, the corresponding wavelength is obtained using (18) as follows:

$$\lambda = \frac{\theta_{el}^{\circ} L_{el}}{60} \leq \frac{11.41 \times 0.17}{60} \leq 0.0323 \text{ m.}$$

As a result, the allowable frequency band should be greater than  $f \geq c_0/\lambda \geq 9.28$  GHz. Therefore, X and Ku frequency bands should be considered for operating radar frequency here.

2) *Radio Signals' Attenuation in Atmosphere*: The received power from a target, in addition to dependence on parameters such as transceiver antenna gain, transmitter power, and target RCS, also depends on the propagation loss. This loss is increased by increasing operating radar frequency. Fig. 3 shows the two-way attenuation coefficients in different radar frequencies. For example, in X-band, the two-way propagation loss is 0.025 dB/km. For a maximum range of 34 km, the propagation loss will be 0.85 dB [21]. In atmospheric conditions (such as rain, snow, and foggy weather), the worsening rate for propagation loss in higher frequencies would be more. For example, in rain at a rate of 3 mm/h, two-way propagation loss for Ku-band will be about 2 dB more than X-band. As the rate of rain and snow is more, the loss is even greater. According to this fact, it can be concluded that the X-band system signal-to-noise-ratio (SNR) would be better than Ku-band.

Another important point is that the targets' RCS variations decrease when radar frequency increases [22]. In this situation, RCS ranges of different surfaces on the ground become closer. Therefore, lower radar frequency conducted in better targets discrimination. Considering all above mentioned fact it is wise to choose frequencies about 9–10 GHz. Additional criterion of frequency choice is the range occupancy by other radio stations. The freest frequencies in 9–10 GHz range are

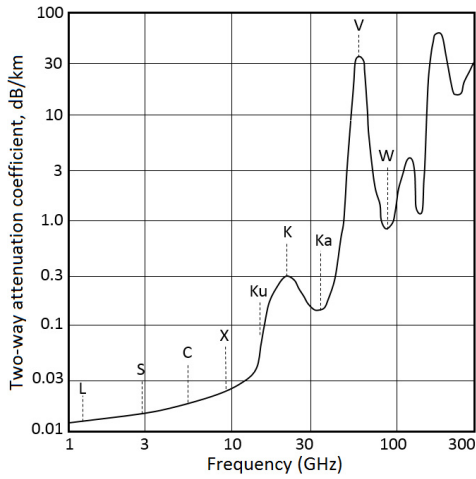


Fig. 3. Two-way attenuation coefficient versus frequency bands [24].

9.3–9.6 GHz. Therefore, these frequencies shall be chosen for SAR operation here.

### B. LFM Bandwidth

Signal bandwidth is specified by resolution requirements. For the initial system requirements given in Table I, the radar ground-range resolution shall be no worse than 10 m in all radar control zone. The 3-dB range resolution,  $\delta_r$  for LFM radar waveform is obtained using  $\delta_r = c_0/(2 \times B)$ , where  $B$  is the bandwidth of probing signal. If probing signal bandwidth is 150 MHz then the resolution element is 1 m. It should be noted that this resolution is provided along the radar beam. The ground-range resolution  $\delta_{gr}$  is inversely proportional to the sinusoid of the grazing angle  $\gamma$ , i.e.,  $\delta_{gr} = \delta_r/\sin \gamma$ . Since the ground surface is surveyed from the missile platform at angles from  $6^\circ$  to  $60^\circ$ , the resolution element width along the ground surface is 1 m divided by sine of angles from  $6^\circ$  to  $60^\circ$ . It will make ground-resolution from 1.15 m to 9.56 m. Base on this fact; it can be concluded that the signal bandwidth 150 MHz is sufficient to meet the requirements.

### C. Synthetic Aperture Length and Accumulation Time

Azimuth resolution is provided by shaping narrow directional pattern in azimuth plane using the synthetic aperture method. It is known that to get the resolution  $d_{az}$  of 1 m, the length of synthetic aperture shall be

$$L_{syn} = \frac{R\lambda}{2d_{az}} \quad (22)$$

where  $R$  is slant range to the resolution element,  $\lambda$  is wavelength,  $d_{az}$  is the resolution along the track.

Since X-band ( $\lambda \approx 3.23$  cm) is chosen for the radar operating frequency, therefore the length of synthetic aperture required to meet the resolution 1 m at maximum slant range of 34 km (flight altitude 30 km) is

$$L_{syn} = \frac{34000 \times 0.0323}{2 \times 0.5} \approx 550 \text{ m.}$$

While aperture synthesis it is required to sum the signals received in spatially spread receiving points and consider the phase within the time of accumulation

$$T_{acc} = \frac{L_{syn}}{v} \quad (23)$$

where  $T_{acc}$  is coherent accumulation time,  $L_{syn}$  is synthetic aperture length, and  $v$  is SAR flight speed.

Therefore the accumulation time for signals reflected from the surface at the maximum range is obtained as  $T_{acc} = 550/2000 = 0.275$  s. At shorter range, the accumulation time decreases, respectively.

### D. Antenna Requirements

Antenna is chosen to meet the following requirements.

- 1) Wavelength is about 3.23 cm (9.3 GHz).
- 2) Elevation directional pattern width (across the aircraft flight) must provide control zone of 1 km at the flight altitude of 5 km.
- 3) Azimuth directional pattern width (along the aircraft flight) shall provide flare of the surface with the length not shorter than the antenna synthetic aperture.
- 4) Maximum gain considering limitations listed above.

Taking into account all the requirements above, the most effective option is microstrip phased array antenna. Microstrip array antennas are utilized in different microwave communication applications because of its attractive features consisting of low profile, light weight, easy fabrication, and adaptation to mounting hosts. In the following, the parameters needed for the antenna system design is presented. It is known that the antenna gain with geometric area of  $A_a$  and efficiency coefficient  $\rho$  is obtained as [21]

$$G = \frac{4\pi\rho A_a}{\lambda^2} = \frac{4\pi A_e}{\lambda^2} \quad (24)$$

where  $A_e$  is effective antenna aperture.

For this kind on antenna, the 3-dB antenna beamwidth in elevation and azimuth directions are obtained using (18) and (19). As we have discussed in Section III-A, beamwidth in vertical plane  $\theta_{el}$  with respected altitude defines swath width. When the flight altitude is 5 km, the swath width is about 1 km. To cover this zone the 3 dB beamwidth in elevation plane shall be about  $11.41^\circ$ .

Acceptable maximum antenna array size in horizontal plane is defined by required control zone in azimuth plane. Control zone shall not be smaller than antenna synthetic aperture. Synthetic aperture length is 550 m considering flight speed of 2000 m/s and accumulation time of 0.275 s. The antenna azimuth beamwidth required at the maximum range of 34 km is obtained as

$$\theta_{az} = \frac{L_{syn}}{R} = \frac{550}{34000} \approx 1^\circ. \quad (25)$$

It should be noted that the above values for antenna are approximate and it will depend on the design procedure may

result in deviation of about 10%. It is clear that the approximate antenna gain value from a rectangular plate with this dimensions of the antenna aperture and efficiency ratio of  $\rho = 0.5$  is obtained using the following:

$$G = \frac{4\pi \times \rho \times L_{el} \times L_{az}}{\lambda^2} = \frac{3600 \times 4\pi \times \rho}{\theta_{az}\theta_{el}} \approx 33 \text{ dB}. \quad (26)$$

### E. Polarization

Single polarization mode is proposed for simple classification and ship detection here. It is shown through different studies of ship detection from polarization information that among the classical linear polarizations HH, VV, and HV, the polarization HH gives the best ship-sea contrast at different grazing angles, even though the sea clutter is the lowest for the HV polarization. However, circular polarizations (CPs) perform better than the HH polarization at lower incidence angles [23].

Linear polarization is very simple to generate but CP is broadly used in many microwave applications. This is because CP exhibits multiple benefits over linear polarization.

- 1) CP avoids polarization losses due to misalignment.
- 2) It has the ability to decrease interference between direct and reflected signal due to multipath propagation.
- 3) CP has the advantage of compactness and low power requirement [24].

Considering all above-mentioned fact it is wise to choose CP for microstrip antenna here.

### F. Pulse Width and PRF

As the radar moves along the imaging area, chirp pulses are transmitted at some constant PRF. The platform motion, the antenna directing, and the antenna beamwidth determine the Doppler frequencies of the echoed signals from the targets in the illuminated area (the Doppler bandwidth). The maximum Doppler frequency cannot be greater than the Doppler bandwidth of the system, defined by the PRF, otherwise Doppler aliasing occurs. Therefore, the lower PRF limit is determined by Doppler bandwidth as

$$\text{PRF}_{\min} = 2 \times \Delta f_d = 2 \times \frac{v \sin(\theta_{az})}{\lambda} \quad (27)$$

where  $\Delta f_d$  is the Doppler bandwidth,  $v$  is missile velocity, and  $\lambda$  is wavelength.

Using (27) and the parameters values obtained in the above discussion, we can obtain the lower limit for PRF which is  $2 \times 2000 \times \sin(1)/0.0323 \approx 2161$  Hz. In addition, the upper PRF limit is determined by the range ambiguities as

$$\text{PRF}_{\max} = \frac{c_0}{2 \times R_{un}} \quad (28)$$

where  $R_{un}$  is the unambiguous range and  $c_0$  is the light speed.

If we consider here that the unambiguous range is the range that the echoed signal is 10 dB lower than the echoed signal from maximum range, i.e.,  $R_{un} = 10^{1/4} 34 \text{ km} \approx 60 \text{ km}$ , it gives the upper PRF limit, 2500 Hz. However, the lower

and upper limits for PRF can be changed as the velocity and maximum range change during the missile flight; therefore an adaptive PRF and PW can be used.

The choice of signal PW is stipulated by requirements for sufficient SNR. The longer signal decreases the duty ratio and therefore increases the average power. The increase of average power leads to the increase of SNR and provides good image on long ranges. At the same time, the PW is limited by pulse repetition interval (PRI). The lower limit for pulse width is determined by minimum range,  $\text{PW} \leq 2 \times R_{\min}/c_0$ , and at the same time the PW is limited by the maximum range and PRI,  $\text{PW} \leq \text{PRI} - 2 \times R_{\max}/c_0$ . Therefore, we can adaptively select the proper value for the PW using following:

$$\text{PW} = \min(2 \times R_{\min}/c_0, \text{PRI} - 2 \times R_{\max}/c_0). \quad (29)$$

For example, if the PRF selected as 2161 Hz,  $R_{\min}$  is 5000 m, and  $R_{\max}$  is 6000 m, therefore the PW will be  $\min(33 \mu\text{s}, 462 \mu\text{s} - 40 \mu\text{s})$ , which is  $33 \mu\text{s}$ . Considering all above-mentioned fact it is wise to choose adaptive PRF and PW using (27) and (29), respectively.

### G. Dynamic Range

The dynamic range of a SAR system is determined based on the various types of earth terrain to be imaged consisting of ocean, sea-ice, man-made target, natural vegetation and agriculture, forest, mountain, and land and sea boundary. The typical value of  $\sigma^0$  falls in the range of +20 dB to -40 dB as mentioned in [25]. In our system, a dynamic range of 40 dB is targeted from +20 dB to -20 dB in order to facilitate the measurement of sea surface and different ships.

### H. Motion Measurement System

Because of the high velocity of the missile and short time of imaging, one can approximate the flight trajectory with a straight line. At least two points are needed in order to estimate a straight line during the imaging time. Based on the time of accumulation formula in (23), at slant range about 6 km, there is approximately 0.1 s time for imaging. Therefore, the GPS/INS rate should be at least 20 Hz in order to give us two samples for flight trajectory estimation. However, because of the error in navigation measurements, it is suggested to have more samples for a better estimation using linear regression (e.g., 100 Hz).

### I. Sampling Frequency and Data Rate

The Nyquist criterion states that in order to construct a band-limited signal from its samples, the signal must be sampled at least twice the highest frequency. In practice, the signal is over-sampled at a rate higher than the Nyquist by 25% in order to account for nonideal filter behavior. In our design, I/Q sampling with the rate of 200 MHz is chosen. The data acquisition unit should start sampling at time of return from minimum range and stop sampling at end of return from maximum range in order to record all the necessary data during the flight. Assuming the aircraft flies at  $R_{\min}$  of 5000 m, and  $R_{\max}$  of 6000 m. PRF is 2161 Hz and PW is selected as  $33 \mu\text{s}$ . The data window is given by time

of flight far range minus time of flight near range plus pulse duration, and is equal to  $6.66 \mu\text{s}$ . Thus the data rate for single ADC channel will be  $(PW + \tau_{\max} - \tau_{\min}) \times f_s$ , which is 7932 samples/echo. Therefore, the total data rate can be calculated by multiplying the data rate with the PRF and the number of bits (assuming 8 bits per sample) which is equal to 137.12 Mb/s.

### J. Transmitted Power

The transmitted signal should have enough power so that the SNR is large enough to generate an appropriate image. The received power at the antenna port for a single radar pulse is associated to the transmitted power as [26]

$$P_r = P_t \frac{G^2 \lambda^2 \sigma}{(4\pi)^3 R^4 L_{\text{radar}} L_{\text{atmos}}} \quad (30)$$

where  $P_t$  is the transmitted signal power (W),  $P_r$  is the power intercepted by the receiver (W),  $G$  is the gain of the antenna in the direction of the target,  $R$  is the range from the antenna to the scatterer (m),  $\sigma$  is the target's radar RCS ( $\text{m}^2$ ),  $\lambda$  is the wavelength of the radar signal (m),  $L_{\text{radar}}$  is the microwave transmission loss factor, and  $L_{\text{atmos}}$  is the atmospheric loss factor due to the propagating wave.

In order to derive the appropriate formula in SAR case, we should replace the RCS for a single target with a distributed RCS multiplied by the area of interest, i.e., a single resolution cell

$$\sigma = \sigma^0 \delta_{\text{az}} \delta_{\text{gr}}. \quad (31)$$

Using (31), we can rewrite (30) as

$$P_r = P_t \frac{G^2 \lambda^2 \sigma^0 \delta_{\text{az}} \delta_{\text{gr}}}{(4\pi)^3 R^4 L_{\text{radar}} L_{\text{atmos}}}. \quad (32)$$

This is the power at the receiver due to the reflection from a target of area  $\delta_{\text{az}} \delta_{\text{gr}}$  having a distributed RCS of  $\sigma^0$ . The effective noise power at the antenna is approximately specified by

$$P_N = kT_0 B F \quad (33)$$

where  $k$  is Boltzmann's constant ( $1.38 \times 10^{-23} \text{ J K}^{-1}$ ),  $T_0$  is the absolute temperature (290 K),  $B$  is receiver bandwidth, Hz, and  $F$  is receiver noise figure.

Consequently, the SNR at the received antenna port is effectively obtained using the following:

$$\text{SNR}_{\text{antenna}} = \frac{P_r}{P_N} = P_t \frac{G^2 \lambda^2 \sigma^0 \delta_{\text{az}} \delta_{\text{gr}}}{(4\pi)^3 R^4 kT_0 B F L_{\text{radar}} L_{\text{atmos}}}. \quad (34)$$

The signal processing for image formation increases the SNR in the SAR image by two main gain factors. The first is because of pulse-compression, and the second is because of coherently accumulating echoes from multiple pulses. This results in

$$\begin{aligned} \text{SNR}_{\text{image}} &= \text{SNR}_{\text{antenna}} G_{\text{az}} G_r \\ &= P_t \frac{G^2 \lambda^2 \sigma^0 \delta_{\text{az}} \delta_{\text{gr}} G_{\text{az}} G_r}{(4\pi)^3 R^4 kT_0 B F L_{\text{radar}} L_{\text{atmos}}} \end{aligned} \quad (35)$$

TABLE II  
SYSTEM PARAMETERS FOR CALCULATING TX POWER

Parameter	Value
Bandwidth (B)	150 MHz
Receiver Noise Figure (F)	4 dB
Antenna Gain (G)	33 dB
Wavelength ( $\lambda$ )	0.0323 m
Maximum Range ( $R_{\max}$ )	34000 m
PRF	2161 Hz
Pulse Length (PW)	33 $\mu\text{s}$
Atmospheric Losses ( $L_{\text{atmos}}$ )	neglected
Radar/Cable Losses ( $L_{\text{radar}}$ )	2 dB
Ground-Range Resolution ( $\delta_{\text{gr}}$ )	10 m
Cross-Range Resolution ( $\delta_{\text{az}}$ )	1 m
RCS ( $\sigma_{\min}^0$ )	-20 dB
Number of Integrations (N)	595

where  $G_r$  is SNR gain due to range processing, and  $G_{\text{az}}$  SNR gain due to azimuth processing.

The range processing gain is because of noise bandwidth reduction during the pulse-compression step. It is straightforward to show that

$$G_r = \frac{\text{PW} \times B}{L_r} \quad (36)$$

where PW is the radar pulse width of the radar and  $L_r$  is the reduction in SNR gain due to nonideal range filtering. Typically  $L_r \approx a_{\text{wr}} \approx 1.2$  or so, where  $a_{\text{wr}}$  is the range impulse response broadening factor due to data weighting or windowing.

The azimuth processing gain is because of the coherent integration of multiple pulses, whether by presumming or azimuth compression. Assuming a broadside collection geometry, and putting all this together yields

$$G_{\text{az}} = \frac{N}{L_a} = \frac{T_{\text{acc}} \text{PRF}}{L_a} \quad (37)$$

where  $N$  is the total number of pulses integrated,  $T_{\text{acc}}$  is the accumulation time obtained in (33), and  $L_a$  is the reduction in SNR gain due to nonideal azimuth filtering. Typically  $L_a \approx a_{\text{wa}} \approx 1.2$  or so.

As we have considered 40 dB dynamic range, therefore, the SNR should be more than 40 dB in the final SAR image after signal processing. Considering all above-mentioned fact, we can find the required transmitted power using the following:

$$P_t = \frac{\text{SNR}_{\text{image}} (4\pi)^3 R_{\max}^4 kT_0 B F L_{\text{radar}} L_{\text{atmos}}}{G^2 \lambda^2 \sigma_{\min}^0 \delta_{\text{az}} \delta_{\text{gr}} G_{\text{az}} G_r}. \quad (38)$$

The expected transmitted power for the missile-borne SAR system can now be calculated using the parameters listed in Table II as

$$\begin{aligned} P_t &= 40 + 3.(10.99) + 4.(45.31) - 262.17 + 24.62 + 81.76 \\ &\quad + 4 + 2 - 2.(33) + 2.(14.9) + 20 - 10 - 27.74 + 1.2 \\ &\quad - 36.94 + 1.2 = 15.94 \text{ dB} \approx 40 \text{ W}. \end{aligned}$$

Finally, the overall missile-borne SAR system parameters are summarized in Table III.

TABLE III  
PROPOSED MISSILE-BORNE SAR SYSTEM CHARACTERISTICS

Parameter	Value
Carrier frequency	9.3 GHz
LFM Bandwidth (B)	150 MHz
Antenna Beamwidth ( $\theta_{el}$ )	11.41°
Antenna Beamwidth ( $\theta_{az}$ )	1°
Antenna Gain (G)	33 dB
Polarization	CP
PRF	2161 Hz or adaptive
Pulse Length (PW)	33 $\mu$ s or adaptive
Dynamic Range	40 dB
Sampling Frequency (1/Q)	200 MHz
Data Rate (b/second)	$(PW + \tau_{max} - \tau_{min}) \times f_s \times 8 \times PRF$
Transmitted power	40 W

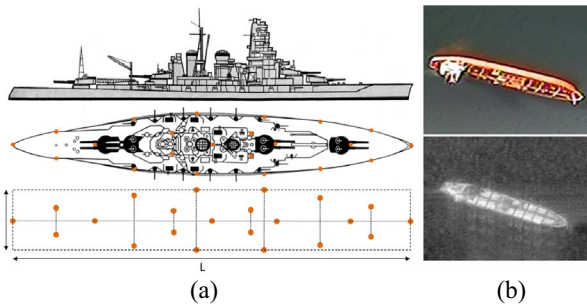


Fig. 4. (a) Warship model for raw signal simulation ( $L = 100$ ,  $W = 25$ ). (b) Top: sample SAR image of a ship at sea with corresponding visual image.

TABLE IV

FLIGHT PARAMETERS OF MISSILE USED IN THE RAW DATA SIMULATION

Parameter	Value
Initial Velocity (see Fig. 2)	(8, 2000, -10) m/s
Acceleration	(3, 2, -9.8) m/s <sup>2</sup>

#### IV. EXPERIMENTAL RESULTS

To quantitatively support the design of SAR seeker and to test processing algorithm, SAR raw-signal simulation is required, particularly when real raw data are not available yet. A model of warship with 22-point targets on it is used to simulate raw SAR signal as shown in Fig. 4(a). To demonstrate the validity of this type of modeling, a sample SAR image of a ship at sea is shown in Fig. 4(b) along with the visual image of it. It can be seen from this figure that the ship is easily recognizable as bright spots against the background of the sea. We have used the traditional time-domain method of raw signal generation in this experiment.

Table IV shows the flight parameters of missile used in the raw data simulation. As it was mentioned in Section I, in the case of imaging in forward- and backward-looking direction for monostatic SAR, left/right ambiguity occurs. Accordingly, we will first simulate a forward-looking scenario using the proposed missile-borne SAR. In this simulation, the missile is at the altitude of 20 km and the ship is at the coordinates of (5002, 1000) on the right side of the missile on the ground. Fig. 5(b) shows the resulted image using the processing algorithm described in Section II. As it can be seen from the result, the ship is visible in both side of the missile; this is called left/right ambiguity.

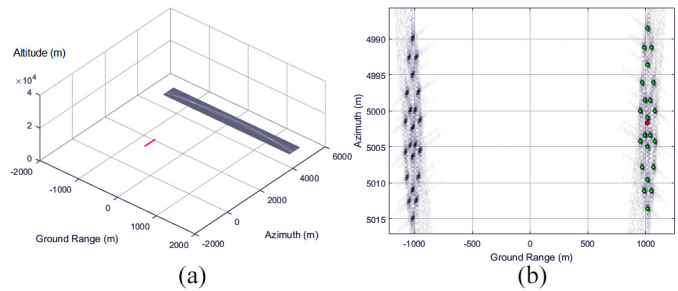


Fig. 5. Left/right ambiguity in forward-looking missile-borne SAR imaging. (a) Missile trajectory (red line) and resulted image on the ground and (b) ship image on the ground (green dots demonstrate the true location of the ship on the right side of the missile).

TABLE V

OBJECTIVE RESULTS RELATED TO THE POINT TARGETS SHOWN IN FIG. 7 (EACH SAMPLE IN AZIMUTH DIRECTION IS EQUAL TO 0.15 m, AND IN GROUND RANGE DIRECTION IS 0.49 m)

T	PSLR <sub>dB</sub>		ISLR <sub>dB</sub>		IRW <sub>sample</sub>		2D-ISLR <sub>dB</sub>
	G.R.	Az.	G.R.	Az.	G.R.	Az.	
1	-32.9	-24.6	-30.6	-12.1	5.52	0.94	-16.4
2	-36.4	-24.8	-29.0	-14.1	10.90	0.92	-18.3
3	-44.6	-24.4	-34.4	-11.7	17.22	0.94	-16.7
4	-35.6	-36.1	-31.9	-22.0	6.00	0.92	-19.6
5	-44.0	-33.1	-35.3	-13.6	12.50	0.85	-15.7
6	-40.1	-40.8	-34.5	-27.3	19.42	0.90	-18.6
7	-24.7	-14.1	-24.2	-8.23	6.92	1.71	-14.4
8	-28.8	-14.6	-26.6	-8.23	14.29	1.76	-14.9
9	-30.5	-14.3	-25.8	-8.01	20.26	1.73	-14.2
10	-23.2	-14.1	-22.4	-8.26	7.52	2.20	-13.8
11	-27.2	-14.6	-25.2	-7.96	15.47	2.06	-14.0
12	-30.4	-15.4	-24.1	-7.13	22.74	2.15	-13.9
13	-21.7	-14.6	-20.3	-8.57	7.92	2.57	-12.1
14	-26.7	-14.5	-22.8	-8.16	16.89	2.30	-13.7
15	-29.1	-14.9	-21.3	-8.46	25.63	2.68	-14.1

As we have mentioned that one simple solution to avoid left/right ambiguity is to use the monostatic SAR in squint mode in order to cover forward direction as much as possible and enlarge the search area for missile. In the following, we have presented the results of stripmap squint mode scenario with different missile-ship configurations.

Fig. 6(a)–(e) shows the simulation results in 15 different missile-ship configurations at five different flight altitudes. It should be noted that in these results, green dots reflect the correct location of the ship and red dots indicate the center of the ship. In addition, Table V shows the objective results related to the point targets shown in Fig. 7. These point targets are the center targets of ship shown in Fig. 6. Four different measures including peak-sidelobe-level-ratio (PSLR), integrated-sidelobe-level-ratio (ISLR), impulse response width (IRW), and 2-D ISLR are used to demonstrate the focusing quality of point targets in different scenarios.

It can be seen from the results that the proposed missile-borne SAR seeker is capable of imaging and positioning the target in different missile-ship configurations at different flight altitudes. However, in the case of extreme squint angles as we have discussed in Section I, the Doppler and ground-range resolutions are extremely low. In one hand, since the gradient of the Doppler frequency in the flight direction is very small,

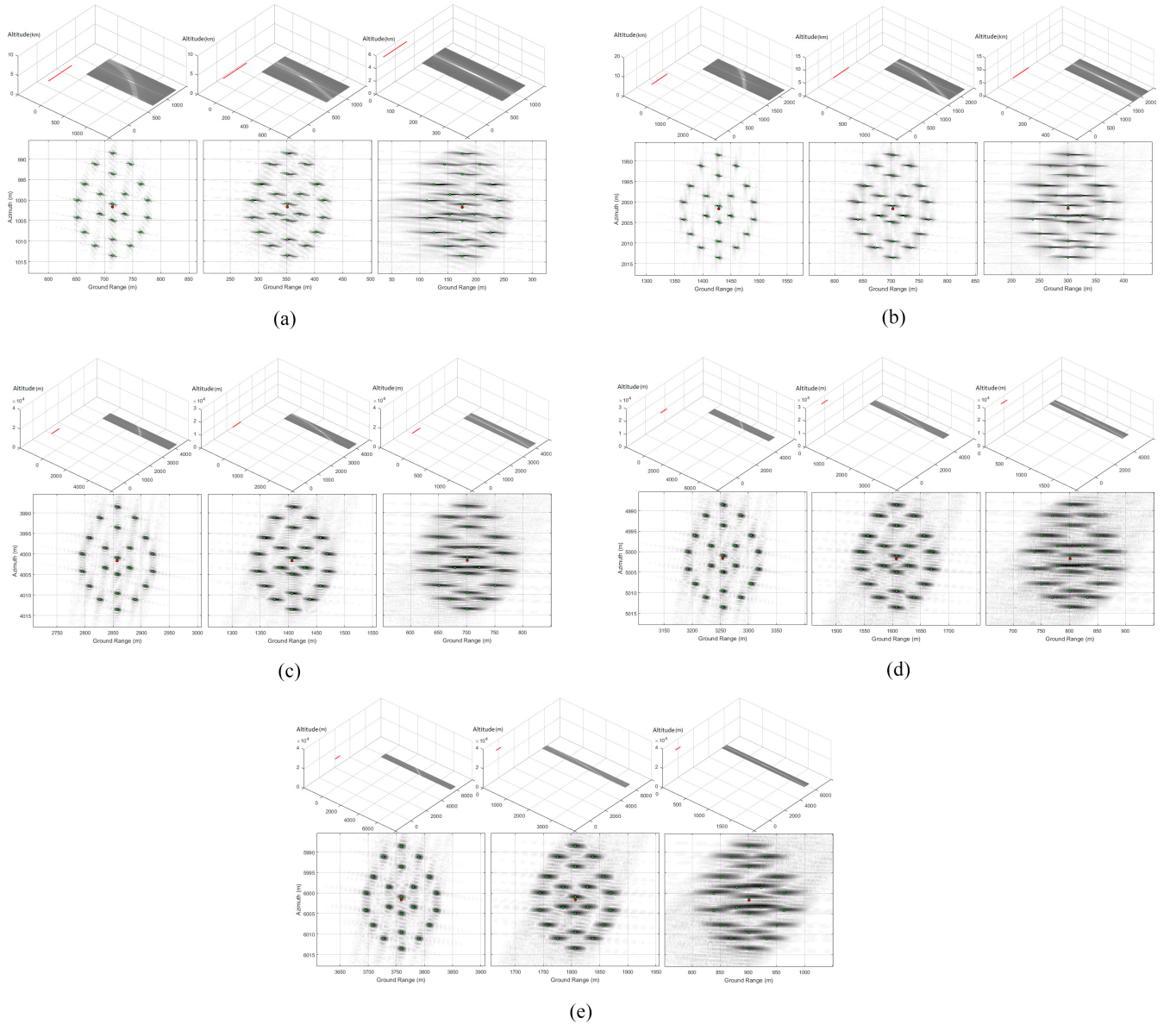


Fig. 6. (a)–(e) Results of missile-borne SAR scenario with different missile-ship configurations, top row: missile trajectory (red line) and resulted image on the ground, and bottom row: ship image on the ground,  $\theta_{sq} \approx 11.25$ .

the Doppler resolution obtained is therefore extremely low. On the other hand, the ground-range resolution is inversely proportional to the sinusoid of the grazing angle; therefore, it will be worsen in angles near to nadir direction. Nonetheless, the resolution issue for missile-borne SAR seeker is not as much problematic as compared to the conventional high-resolution SAR imaging. This is because the missile-borne SAR seeker is considered here in the context of positioning and targeting sea targets as opposed to high-resolution imaging. It can be seen from the results that in the case of extreme squint angles, the proposed missile-borne SAR seeker is capable of positioning the ship on the ground with small errors. It should be mentioned that after the ship detection step, the missile must appropriately move toward the target in the track mode to able the SAR seeker for producing good resolution images. In order to get the best resolution, the missile curve trajectory

must be designed and optimized. However, this is beyond the scope of this paper.

Another problem that should be considered here is the effect of warship target motion in missile-borne SAR system. For this reason, a Doppler term has been added to the received signal model in (5) for raw signal generation as follows:

$$s'_{rm}(t, \eta) = \exp(jf_d(t, \eta)) \cdot s_{rm}(t, \eta) \quad (39)$$

where  $f_d$  is obtained as follows:

$$f_d(t, \eta) = 2\pi \left( \frac{2v_{sh}}{\lambda} \right) \sin(\theta_{az}(t, \eta)) T_f(t, \eta) \quad (40)$$

where  $v_{sh}$  is warship velocity,  $\theta_{az}$  is the instantaneous angle between the platform and the target, and  $T_f$  is time of flight during the imaging.

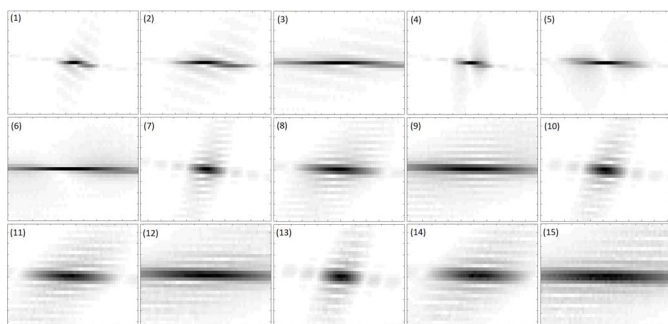


Fig. 7. Point target responses at the center of warship model in 15 different missile-ship configurations at five different flight altitudes as shown in Fig. 6.

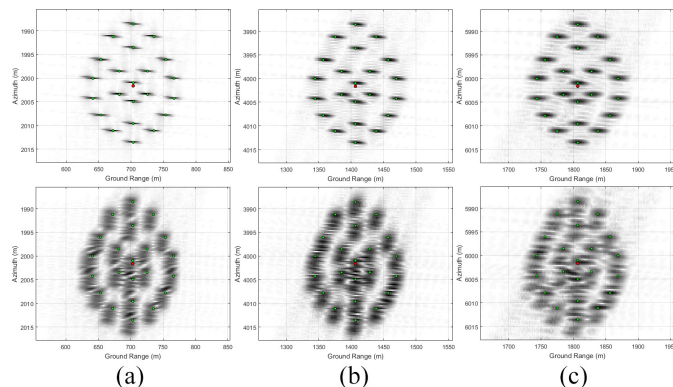


Fig. 8. Results of stripmap squint mode missile-borne SAR scenario considering ship motion effect at different missile altitudes. (a) 10 km. (b) 20 km. (c) 30 km. Top row: without motion, and bottom row: with motion.

In this simulation, a speed of 22.5 knot (26 mph/42 kph) is selected for warship velocity, which is usually considered a high-speed in the sea. Three different scenarios with different missile-ship configurations has been selected for showing the effect of warship motion during SAR imaging. The result is depicted in Fig. 8. As it could be expected, the phase error in SAR signal due to the target motion causes imperfect focusing in reconstructed SAR image. Obviously, the image resolutions are degraded in both directions. However, the center location that is the main objective of a seeker can still be determined with good quality as it can be seen in the results.

## V. CONCLUSION

In this paper, feasibility study along with conceptual design of missile-borne SAR seeker has been performed, which can effectively improve the detection capability and the blow precision of a missile. Signal modeling, image formation algorithm, and system design considerations are discussed in this paper. In addition, simulation of whole system along with raw data generation considering the imaging geometry of missile-borne SAR seeker has been performed. As a conclusion, we can mention the following.

- 1) SAR is the only effective sensor capable of operation on a day/night basis and in all weathers and it has a high imaging resolution.
- 2) Since the RCS of ships and sea are very different, ships in a SAR image are easily recognizable as bright spots.

As a result, SAR sensor can be considered as one of the best options for antiship ballistic missile seeker.

- 3) Feasibility study and system design considerations indicate that SAR system can be used with high reliability as missile's seeker.
- 4) The experimental results show that the proposed missile-borne SAR seeker in the case of extreme squint angles is capable of imaging and positioning target like ship in sea area.

For future work, we will investigate different methods for missile's trajectory optimization (after the ship detection step, the missile must appropriately move toward the target to able the SAR seeker for producing good resolution images) and other image processing algorithms for image formation with lower computation complexities.

## ACKNOWLEDGMENT

The author would like to thank the anonymous reviewers for their helpful and constructive comments that greatly contributed for improving this paper.

## REFERENCES

- [1] J. Saeedi, "Synthetic aperture radar signal processing using nonlinear frequency modulation and phase error compensation," Ph.D. dissertation, Dept. Elect. Eng., Amirkabir Univ. Technol., and Tehran Polytech., Tehran, Iran, 2015.
- [2] J. Saeedi and S. M. Alavi, "Improved navigation-based motion compensation for LFM CW synthetic aperture radar imaging," *Signal Image Video Process.*, vol. 10, no. 2, pp. 405–412, 2016.
- [3] Z. S. Ming, C. Y. Ying, and L. Yi, "A robust matching algorithm for SAR image with multiple sub-areas," *Acta Geodaetica et Cartographica Sinica*, vol. 36, no. 4, pp. 406–413, 2007.
- [4] H. Zhi-Ming, Z. Jiang, and Z. Bo, "Research on real-time signal processing of the missile-borne SAR," *J. Electron. Inf. Technol.*, vol. 30, no. 4, pp. 1011–1013, 2008.
- [5] The Small Business Innovation Research. (1987). *High Altitude Synthetic Aperture Radar (SAR) for Ballistic Missile Missions*. [Online]. Available: <https://www.sbir.gov/sbirsearch/detail/143554>
- [6] Federation of American Scientists. (2015). *AGM-158 Joint Air to Surface Standoff Missile (JASSM)*. [Online]. Available: <http://fas.org/man/dod-101/sys/smart/jassm.htm>
- [7] E. Hagt and M. Durnin, "China's antiship ballistic missile," *Naval War College Rev.*, vol. 62, no. 4, pp. 87–116, 2009.
- [8] B. Deng, X. Li, H. Wang, Y. Qin, and J. Wang, "Fast raw-signal simulation of extended scenes for missile-borne SAR with constant acceleration," *IEEE Geosci. Remote Sens. Lett.*, vol. 8, no. 1, pp. 44–48, Jan. 2011.
- [9] A. Farooq and D. N. Limebeer, "Optimal trajectory regulation for radar imaging guidance," *J. Guid. Control Dyn.*, vol. 31, no. 4, pp. 1076–1092, 2008.
- [10] T. J. Peregriam, F. A. Okurowski, and A. H. Long, "Synthetic aperture radar guidance system and method of operating same," U.S. Patent 543 044 5A, 1995.
- [11] I. J. H. Ender, *Introduction to Radar—Part I*, document, Script Lecture Ruhr-Universität Bochum, Bochum, Germany, 2011.
- [12] D. Wei, Z. Ming-Bo, and Z. Dong-Xing, "Target reference template generation techniques for homing guidance by radar scene matching," in *Proc. 10th Acad. Conf. Radar*, Beijing, China, 2008, pp. 1352–1354.
- [13] S. Minaeian, J. Liu, and Y.-J. Son, "Vision-based target detection and localization via a team of cooperative UAV and UGVs," *IEEE Trans. Syst., Man, Cybern., Syst.*, vol. 46, no. 7, pp. 1005–1016, Jul. 2016.
- [14] L. Shen, C.-J. Jiang, and G.-J. Liu, "Satellite objects extraction and classification based on similarity measure," *IEEE Trans. Syst., Man, Cybern., Syst.*, vol. 46, no. 8, pp. 1148–1154, Aug. 2016.
- [15] W. Cao, J. Lan, and X. R. Li, "Conditional joint decision and estimation with application to joint tracking and classification," *IEEE Trans. Syst., Man, Cybern., Syst.*, vol. 46, no. 4, pp. 459–471, Apr. 2016.

- [16] Z. Hongzhong, X. Huaying, and F. Qiang, "Azimuth resolution acquisition through trajectory optimization for a SAR seeker," in *Proc. 2nd Asian-Pac. Conf. Synthetic Aperture Radar*, Xi'an, China, 2009, pp. 55–59.
- [17] C. Anagnostopoulos and S. Hadjiefthymiades, "Intelligent trajectory classification for improved movement prediction," *IEEE Trans. Syst., Man, Cybern., Syst.*, vol. 44, no. 10, pp. 1301–1314, Oct. 2014.
- [18] W. Yuan, Y. Liu, H. Wang, and Y. Cao, "A geometric structure-based particle swarm optimization algorithm for multiobjective problems," *IEEE Trans. Syst., Man, Cybern., Syst.*, to be published.
- [19] J. Saeedi and K. Faez, "Synthetic aperture radar imaging using nonlinear frequency modulation signal," *IEEE Trans. Aerosp. Electron. Syst.*, vol. 52, no. 1, pp. 99–110, Feb. 2016.
- [20] J. Saeedi and K. Faez, "A back-projection autofocus algorithm based on flight trajectory optimization for synthetic aperture radar imaging," *Multidimensional Syst. Signal Process.*, vol. 27, no. 2, pp. 411–431, 2016.
- [21] C. R. Jackson and J. R. Apel, "Synthetic aperture radar marine user's manual," U.S. Dept. Commerce, Washington, DC, USA, Tech. Rep., 2004. [Online]. Available: <http://www.sarusersmanual.com/>
- [22] J. B. Billingsley, *Low-Angle Radar Land Clutter*. Norwich, U.K.: William Andrew, 2002.
- [23] S. Angelliaume, P. Martineau, P. Durand, and T. Cussac, "Ship detection and sea clutter characterisation using X&L-band full-folarimetric airborne SAR data," in *Proc. SeaSAR*, Tromsø, Norway, 2012, pp. 1–4.
- [24] J. T. Sri-Sumantyo, "Development of circularly polarized synthetic aperture radar (CP-SAR) onboard small satellite," in *Proc. PIERS*, Marrakesh, Morocco, 2011, pp. 334–341.
- [25] J. T. Pulliainen, K. Heiska, J. Hyypä, and M. T. Hallikainen, "Backscattering properties of boreal forests at the C- and X-bands," *IEEE Trans. Geosci. Remote Sens.*, vol. 32, no. 5, pp. 1041–1050, Sep. 1994.
- [26] F. T. Ulaby, R. K. Moore, and A. K. Fung, *Microwave Remote Sensing: Active and Passive*. Norwood, MA, USA: Artech House, 1981.



**Jamal Saeedi** (M'01) received the B.Sc. degree in biomedical engineering from the Sahand University of Tabriz, Tabriz, Iran, in 2007 and the M.Sc. and Ph.D. degrees in electronic engineering from the Amirkabir University of Tehran, Tehran, Iran, in 2010 and 2015, respectively.

He has over 18 publications in various areas, including signal and image processing, radar, and synthetic aperture radar. His current research interests include signal and image processing, specializing particularly in information fusion, pattern recognition, road traffic monitoring systems, and synthetic aperture radar signal processing.